# Study of Solar Cells Using FISH MOSFETs as a Constructive Element to Generate Photocurrent in the Longitudinal Direction

Fernando Pizzo Ribeiro[1], Egon Henrique Salerno Galembeck[2], Rodrigo Alves de Lima Moreto[2] and Salvador Pinillos Gimenez[1]

[1]Electrical Engineering Department, University Center FEI, São Bernardo do Campo, Brazil
[2]MTG2i Solutions Co, São Bernardo do Campo, Brazil
e-mail: egon@mtg2isolutions.com, ferpizzo@fei.edu.br, sgimenez@fei.edu.br

***Abstract*— According to a study by the International Energy Agency (IEA), solar energy could reach 30% in 2023 in countries with the most excellent installed generation capacity, such as China, Germany, Japan, and the United States of America. In other countries, like Brazil (mainly in Paraiba state), for instance, the volume of investments in the solar energy sector is equal to 4.17 billion Reais of private investments in 2022 to implement a photovoltaic module factory to reach an installed capacity of 1.6GW. In this context, several efforts have been made to boost the electrical performance of solar cells in terms of using new materials, fabrication processes, and constructive essential elements to produce electric energy with more efficiency. Thus, this paper performs, by three-dimensional numerical simulations, a comparative study between solar cells implemented with constructive elements based on Metal-Oxide-Semiconductor Field Effect Transistors (MOSFETs), N channel, depletion type, with two types of gate geometries, in which one is layouted with the typical rectangular (Rectangular MOSFET, RM) and other is implemented with the FISH layout style (FISH MOSFET, FM). The main results have shown that the solar cell implemented with the FISH MOSFET has an efficiency of approximately 57% higher than that presented in the solar cell implemented with the Conventional MOSFET. Therefore, the solar cells implemented with FISH MOSFETs can be considered an alternative constructive essential element to improve the electrical performance of solar cells.**

***Index Terms* - Solar cell; MOSFET; FISH layout style; Longitudinal Corner Effect, 3D numerical simulations.**

## I. Introduction

According to a study by the International Energy Agency (IEA), solar energy could reach 30% in 2023 in countries with the most significant electricity generation capacity, such as China, Germany, Japan, and the United States of America (USA). For instance, in 2016, Japan expanded its installed capacity and became the second country that most uses solar (photovoltaic) energy globally, producing 42,750 MW of electricity. Germany estimates a production of 35% of its electrical energy based on renewable energy sources and seeks to reach 100% by 2050. The USA aims, in 2023, to get the mark of 30% of its electrical energy coming from renewable sources [1], [2]. In Brazil, the volume of private investments in the solar energy sector in June 2021 was 4.17 billion reais in Paraiba state to produce photovoltaic modules and a solar complex with an installed capacity of 1.6 GW. Besides, in 2019, the solar energy market in Brazil has grown more than 212%, reaching the mark of 2.4 GW installed. According to the National Electric Energy Agency (ANEEL), more than 110,000 mini and microgeneration photovoltaic systems were installed in companies, homes, businesses, farms, etc., corresponding to R$ 4.8 billion and more than 15,000 professionals working there. In December 2022, Brazil reached 23 GW of installed solar power, registering an increase of almost 66% in one year. Brazil is expected to add more than 10 GW of solar photovoltaic generation in 2023 and reach an accumulated installed capacity of 34 GW [3].

Several efforts have been made to improve solar cells' electrical performance using new fabrication processes, materials, wafers, and constructive essential elements (diodes, MOSFETs, etc.) [4]–[13]. For instance, the authors Elisa Antolín et al. have studied the concept of a solar cell based on a Hetero-Junction Bipolar Transistor Solar Cell (HBTSC), which is simple, compact, and economical. This cell can provide a higher annual electrical energy yield and is even more versatile for the combination of semiconductor materials than the series-connected multijunction technology currently used [4]. Another study has been performed that uses new technologies to form a more efficient solar cell by using perovskite materials, which have low cost and excellent optoelectronic properties for implementing solar cells. The authors have proposed the development of a silicon-perovskite solar cell based on the three-terminal heterojunction bipolar transistor architecture. To evaluate the potential of this structure, the classic extended Hovel model was used, and efficiencies of up to 28.6% were obtained for cells without anti-reflective coating [5]. The authors Q.R. Lai et al. have demonstrated a new concept for a photovoltaic device using a Metal-Oxide-Semiconductor Field Effect Transistor (MOSFET) with a silicon structure and a transparent gate electrode (Indium Tin Oxide, ITO). This structure also has a solar cell with auxiliary biasing and showed an increase of 12.93% in the photocurrent of the device, as illustrated in Figure 1 [6].

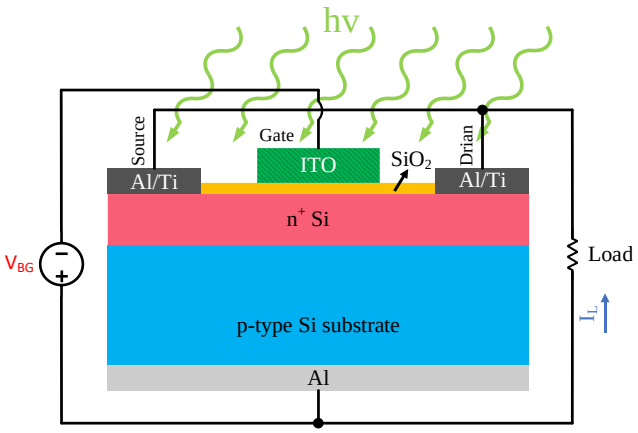


Fig. 1. Photocurrent of MOS-Si Photovoltaic Device Enhanced by an Auxiliary Biasing Solar Cell [6].

In Fig. 1, hv is the incident light energy, Al is aluminum, ITO is the indium tin oxide, Ti is the titanium, $I_L$ is the load current, $n^+$ Si is Silicon's region with a doping concentration

of n-type, $V_{BG}$ is the gate voltage that biases the solar cell, $SiO_2$ is the silicon oxide layer, and Si is the Silicon.

The Metal-Oxide-Semiconductor (MOS) structure consists of a semiconductor substrate, an oxide layer, and a metal contact, as Fig. 1 illustrates. When light hits the semiconductor, it creates electron-hole pairs. The electrons are attracted to the metal contact. At the same time, the holes migrate towards the oxide layer, generating a current that can effectively supply power to electrical devices. MOS solar cells offer numerous advantages compared to other solar cell varieties. They boast a relatively straightforward fabrication process and can be constructed from diverse semiconductor materials, such as silicon, gallium arsenide, and indium gallium phosphide. This versatility makes them an excellent choice for applications where cost-effectiveness and adaptability are paramount. While MOS solar cells offer numerous benefits, they come with disadvantages. They are less efficient than other solar cell varieties and can be susceptible to moisture and heat. Nevertheless, researchers are actively working to mitigate these disadvantages, making MOS solar cells a promising and emerging technology in the field of solar energy generation [6]–[9], [14].

Besides, Mahmudur Siddiqui et al. have researched a new double-gate MOS structure that uses intrinsic silicon as an active material for application in photovoltaic cells. As a great advantage, this device has low recombination of optically generated charge carriers due to the intrinsic nature of the active region, allowing the charge carriers to transit at high speed under the effect of the external electric field. It was found that the proposed device showed higher efficiency and higher open circuit voltage compared to those observed in typical p-n junction solar cells [7], [14].

Researchers from around the world are dedicated to enhancing MOS solar cell performance through the exploration of novel materials and structures. Through ongoing research and development efforts, MOS solar cells promise to contribute to solar energy generation significantly. In this scenario, the main objective of this paper is to perform a comparative study, by three-dimensional (3D) numerical simulations, between solar cells implemented with MOSFETs, n-channel, depletion mode, with conventional rectangular gate shape (Rectangular MOSFET, RM) and FISH layout style (gate shape visually like the mathematical symbol representing the greater than sign, “>”), entitled FISH MOSFET, FM [15]–[17], as constructive elements.

## II. Device’s Characteristics and Structures

Fig. 2 illustrates views of MOSFETs, n-channel, and depletion mode, used as constructive elements of the solar cells, which were layouted with the rectangular (RM) and FISH (FM) layout styles, respectively: top view of RM (a), top view of FM (b), and front view of the cross-section of RM (c).

In Fig. 2, L (0.56 μm) and W (0.81 μm) are, respectively, the channel length and width, α is the angle of the FISH layout style, $n^+$ type Si is the silicon regions of the drain and source ($1x10^{19}$ $cm^{-3}$), p-type Si is the silicon substrate ($1x10^{16}$ $cm^{-3}$), $p^+$ type Si is the silicon regions of the substrate ($5x10^{16}$ $cm^{-3}$), d is the distance between the drain and source regions and $p^+$ type substrate (0.05 μm), $t_{OX}$ é the silicon-oxide thickness (4.2 nm), $t_{Si}$ is the depth of the silicon wafer (1 μm), $t_{p+}$ is the depth of the $p^+$ type Si regions (0.35 μm), $t_{n+}$ is the depth of the $n^+$ type Si regions (0.35 μm), $V_{BG}$ is the gate voltage that biases the solar cell, R is the load resistance (10 Ω), and $V_{BG}$ is the additional power supply to bias the gate region of MOSFETs.

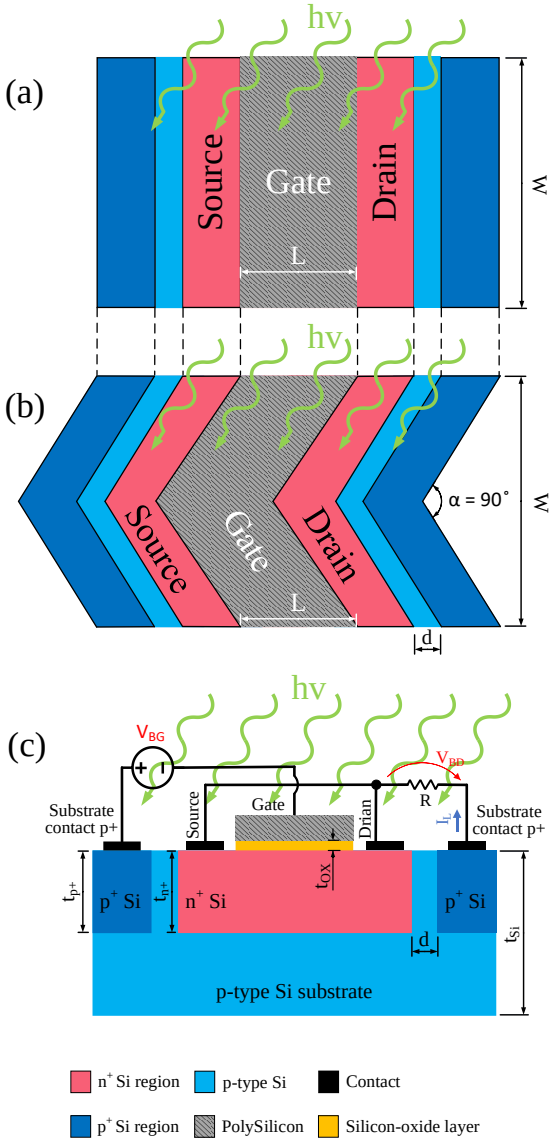


Fig. 2 Views of MOSFETs, n-channel, and depletion mode, with the rectangular (a) and FISH (b) layout styles and the cross-section of the rectangular MOSFET structure used as the constructive essential elements of solar cells (c).

The FM presents in its structure the Longitudinal Corner Effect (LCE) [15]–[17]. This effect can boost the longitudinal electric field along the channel length and enhance the MOSFETs' drain current ($I_{DS}$). This occurs because it generates two longitudinal electrical field components due to the geometric shape that presents two edges (like a mathematical symbol: “<”) instead of only one like RM has [15]–[17].

To perform the three-dimensional (3D) numerical simulations of the structures illustrated in Fig. 2 as the essential elements for implementing a solar cell, an ohmic resistance of 10 Ω was electrically connected between the substrate and drain terminals ($V_{BD}$). Besides, an external

power supply, which can be implemented with another solar cell, is applied in the gate of MOSFETs, n-channel, and depletion mode (Fig. 3). Furthermore, these MOSFETs are irradiated perpendicularly by an AM1.5G spectrum [6], [7].

## III. 3D Numerical Simulations Results And Discussions

This section presents the main results of the electrical characterizations of FM and RM considered in this work, operating as constructive essential elements of solar cells.

To perform the 3D numerical simulation, we have used the Sentaurus 3D Technology Computer-Aided Design (3D TCAD) simulation tool from Synopsys Company [18]. The 3D numerical simulations were explicitly conducted using Silicon. However, the scope of this study could also encompass various other semiconductor materials. The critical physical models used in the 3D numerical simulations were [18]: High field saturation model [19]; Philips Unified Mobility model [20]; Enormal model [21], and Shockley–Read–Hall [22] with sub-model DopingDep [23].

To electrically characterize the solar cell implemented with FM and RM, initially, we have biased the gate voltage ($V_{BG}$), which is defined by the voltage of the external power supply, equal to 0 V. After that, we apply the different wavelengths of the AM1.5G spectrum (from 400 nm to 1800 nm), and we measured the load current ($I_L$), which is equal to the substrate current ($I_B$), and load (R) under voltage $V_{BD}$, which in this case is represented by the potential difference between the substrate region and the drain region that is short-circuited with the source region. After that, we plotted the negative of $I_L$ ($-I_L$) as a function of the $V_{BD}$ of these devices, as indicated in Fig. 3. After that, we proceeded in the same way, i.e., we varied the values of $V_{BG}$ from -5 V to +5 V, with steps of 1 V. Afterward, based on the graphic of $-I_L$ as a function of the $V_{BD}$, we have plotted the electrical power (P), given by the modulus of ($-I_L$) multiplied by $V_{BD}$, as a function of the load voltage ($V_{BD}$), as illustrated in Fig. 3, so that we can characterize the efficiency (η) and Fill Factor (FF), respectively.

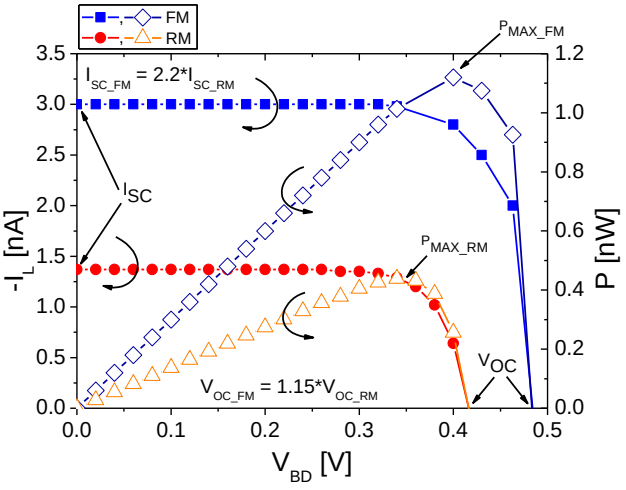


Fig. 3 -$I_L$ and P as a function of $V_{BD}$ of the MOSFETs, n-channel, depletion-type, layouted with the FISH and conventional rectangular layout styles, considering the wavelengths of the AM1.5G spectrum and different $V_G$ (from -5 V to +5 V).

In Fig. 3, $I_{SC\_FM}$ and $I_{SC\_RM}$ are the short-circuit electric currents of FM and RM, respectively, $V_{OC\_FM}$ and $V_{OC\_RM}$ are the open-circuit voltage of FM and RM, respectively, and $P_{MAX\_FM}$ and $P_{MAX\_RM}$ are, respectively, the maximum electric powers of FM and RM.

By analyzing Fig. 3, we have characterized the values of $I_{SC}$ of both MOSFETs, n-type, depletion mode, implemented with FISH and rectangular layout styles, respectively, which are equal to 2.963 nA and 1.388 nA, and the values of $V_{OC}$ of these devices, in which are equal 491 mV to 436 mV, and the values of their maximum electric powers, that were equal to 1.120 nW and 0.436 nW, respectively. Furthermore, we have observed that the characteristic curves of these transistors did not change when we varied the $V_{BG}$ from -5V to +5V, which was defined by the $V_{BG}$ of the additional external power supply. Therefore, we have concluded that using the FISH layout style for MOSFETs, n-channel, depletion mode, as an essential constructive element of a solar cell (photocell), we can boost its electrical characteristic curve in terms of its generation capacity of the electric photocurrent ($-I_L$), the open-circuit voltage ($V_{OC}$), and the maximum electric power ($P_{MAX}$). In our case, the $-I_L$, $V_{OC}$, and $P_{MAX}$ of the solar cell implemented with the FISH layout style are 2.2 times, 15% and 55% higher than those measured of MOSFET, n-type, depletion mode, implemented with the conventional rectangular layout style.

The efficiency of a solar cell (η) is defined by the ratio of the electrical power output of the solar cell ($P_{MAX}$), usually measured in watts (W), and $P_{IN}$ is the total incident power from sunlight on the solar cell, also measured in watts (W), which is calculated by the product of the surface area of the solar cell exposed to sunlight (A), measured in square meters ($m^2$) and the solar irradiance (G), which is the electric power per unit area received from the sun, that is typically measured in watts per square meter ($W/m^2$), considered in this study equal to 1000 $W/m^2$ (Brazil conditions), and it is given by Equation (1) [8], [11], [14].

$$\eta = \frac{P_{MAX}}{P_{IN}} = \frac{P_{MAX}}{A.G} \quad (1)$$

The Fill Factor (FF) is a figure of merit used to characterize the electrical performance of a solar cell or photovoltaic (PV) module, as indicated in Equation (2). It measures how effectively the solar cell can convert sunlight into electrical energy. It is expressed as a decimal or percentage and typically falls from 0 to 1 or 0% to 100% [8], [11], [14].

$$FF = \frac{P_{MAX}}{V_{OC} \cdot I_{SC}} \quad (2)$$

Table II presents the values of $V_{OC}$, $I_{SC}$, $P_{MAX}$, η, and FF of the solar cells implemented with FM and RM, respectively, regarding their incident areas (A) of sunlight equal to 1.5 $\mu m^2$, considering different values of $V_{BG}$.

Table I. The values of $V_{OC}$, $I_{SC}$, $P_{MAX}$, η, and FF for different values of voltage applied to the gate ($V_{BG}$) of FM and RM, respectively.

| | ***FISH MOSFET*** | | | | | ***Rectangular MOSFET*** | | | | |
|---|---|---|---|---|---|---|---|---|---|---|
| ***$V_G$ [V]*** | *$V_{OC}$ [V]* | *$I_{SC}$ [nA]* | *$P_{MAX}$ [nW]* | *η [%]* | *FF [%]* | *$V_{OC}$ [V]* | *$I_{SC}$ [nA]* | *$P_{MAX}$ [nW]* | *η [%]* | *FF [%]* |
| ***-5*** | 0.490 | 2.934 | 1.108 | **36.93** | **77.07** | 0.418 | 1.376 | 0.432 | **14.38** | **75.11** |
| ***-3*** | 0.490 | 2.935 | 1.109 | **36.97** | **77.11** | 0.417 | 1.376 | 0.432 | **14.38** | **75.29** |
| ***-2*** | 0.490 | 2.935 | 1.108 | **36.93** | **77.04** | 0.417 | 1.376 | 0.432 | **14.40** | **75.29** |
| ***-1*** | 0.490 | 2.936 | 1.108 | **36,93** | **77.02** | 0.418 | 1.376 | 0.432 | **14.40** | **75.11** |
| ***0*** | 0.491 | 2.962 | 1.120 | **37.33** | **77.01** | 0.417 | 1.388 | 0.436 | **14.53** | **75.33** |
| ***1*** | 0.491 | 2.963 | 1.120 | **37.33** | **77.00** | 0.416 | 1.388 | 0.436 | **14.54** | **75.51** |
| ***2*** | 0.490 | 2.963 | 1.120 | **37.33** | **77.14** | 0.418 | 1.388 | 0.436 | **14.54** | **75.15** |
| ***3*** | 0.490 | 2.963 | 1.120 | **37.33** | **77.14** | 0.417 | 1.388 | 0.436 | **14.54** | **75.33** |
| ***5*** | 0.490 | 2.963 | 1.120 | **37.33** | **77.14** | 0.417 | 1.388 | 0.436 | **14.56** | **75.33** |

Based on the values presented in Table I, we have observed that the efficiency (η) measured of the solar cell implemented with FM (on average 37.2%), using it as an essential constructive element, is 157% (2.57 times) higher than the one observed in the solar cell implemented by RM (on average 14.5%), regarding the same bias conditions, dimensions, light spectrum (AM1.5G), and intensity of the incident light energy. This result can be justified due to the presence of the LCE effect in its structure, which is responsible for increasing the resultant longitudinal electric field in the depletion regions of the PN metallurgical junctions between drain/source and substrate regions. Besides, the photocurrent ($-I_L$) generated in the load (R) by the photoelectric effect occurs in the wafer's surface, presenting a smaller resistance between drain/source and substrate regions, in contrast to what happens in the typical solar cells (in the vertical direction), according to described in reference [6]. Furthermore, the FF of both solar cells implemented with FM and RM are practically the same (worst case: maximum difference of 2%). This result can be justified because the ratios of $P_{MAX}$ divided by the product of $V_{OC}$ and $I_{SC}$ of both solar cells present practically the same values. This occurs because the solar cell implemented with FM can increase $I_{SC}$ and $V_{OC}$ simultaneously due to the intrinsic LCE effect in its structure. These results are significant because by using the solar cells implemented with the FISH layout style, it is possible to reduce the number of modules that must be electrically connected in parallel to reach the desired voltage of a specified electric system.

Fig. 4 illustrates the Efficiency (η) [Fig.4 (a)] and Fill Factor (FF) [Fig.4 (b)] of the solar cells implemented with FM and RM, respectively, as a function of the external bias voltage applied to the gate terminal ($V_{BG}$), regarding different wavelengths of the AM1.5G spectrum (from 400 nm to 1800 nm) and the same bias conditions.

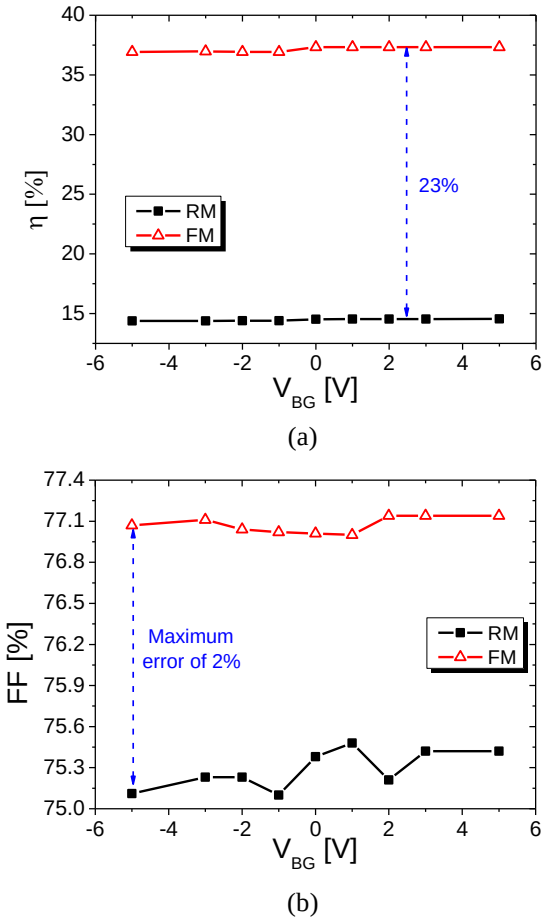


Fig. 4 The Efficiency (a) and Fill Factor (b) as a function of the $VB_G$ of a MOSFET structure solar cell implemented with the FISH and conventional rectangular layout styles concerning different wavelengths of the AM1.5G spectrum (from 400 nm to 1800 nm) and the same bias conditions.

Analyzing the results presented in Fig. 4, we observe that the behaviors of the Efficiencies (η) and Fill Factors (FF) as a function of $V_{BG}$ are practically constants in both solar cells. Therefore, the influence of $V_{BG}$ in the and FF of both solar cells was not significant in further improving their electrical performances (maximum variation of 0.4% of both figures of merit and FF).

To justify the results obtained of the better electrical performance of the solar cell implemented with FM in comparison to the one built with RM counterpart, we have plotted the longitudinal electric field as a function of the length defined from the beginning of the drain region (0 μm) to the end of p+ substrate (0.65 μm), defined as “Distance,” concerning the different wavelengths of the AM1.5G spectrum (from 400 nm to 1800 nm) and the same bias conditions, as illustrated in Fig. 5.

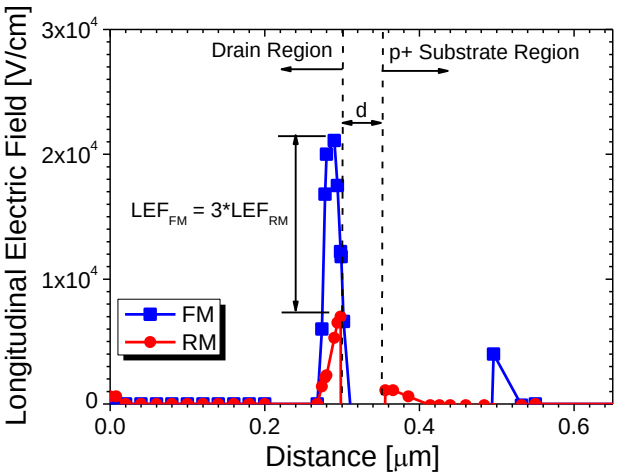


Fig. 5 The Longitudinal Electric Field along the beginning of the drain region (0 μm) to the end of p+ substrate (0.65 μm), concerning different wavelengths of the AM1.5G spectrum (from 400 nm to 1800 nm) and the same bias conditions.

In Fig. 5, $LEF_{FM}$ and $LEF_{RM}$ are, respectively, the longitudinal electric fields along the beginning of the drain region (0 μm) to the end of the p+ substrate (0.65 μm) of the FM and RM structures.

Based on Fig. 5, the $LEF_{FM}$ is three times higher than the $LEF_{RM}$, thanks to the LCE effect in the FM structure, and therefore, the FISH layout style for MOSFETs operating as a solar cell can boost its electrical performance in terms of $V_{OC}$, $I_{SC}$, $P_{MAX}$ and η.

## IV. Conclusion

This paper has performed a comparative study between two solar cells, which are implemented with MOSFETs, n-channel, and depletion mode, regarding two different layout styles (FISH and conventional rectangular) using 3D numerical simulations. The main results were that the FISH layout style could remarkably boost the solar cell's efficiency. In this case, we have found an increase of 157% (2.57 times higher) compared to the solar cell implemented with the conventional rectangular MOSFET, thanks to the Longitudinal Corner Effect (LCE) present in the FISH MOSFET structure. Furthermore, based on this study, we can reduce the number of solar cell modules that must be electrically connected in parallel to reach the desired voltage of a specified electric system by using the solar cells implemented with the FISH layout style due to $V_{OC}$ improvement concerning the one measured in the solar cell implemented with RM. Therefore, using the FISH layout style for MOSFETs to operate as an essential constructive element can be considered an important alternative to boost the electrical performance of solar cells.

## Acknowledgments

This study was financed in part by the Coordenação de Aperfeiçoamento de Pessoal de Nível Superior - Brasil (CAPES) - Finance Code 001. Salvador Pinillos Gimenez acknowledges CNPq (grant #304427/2022-5) for the financial support and Egon Henrique Salerno Galembeck, Rodrigo Alves de Lima Moreto, and Salvador Pinillos Gimenez thank the São Paulo Research Foundation (FAPESP) grant #2020/09375-0 for the financial support.

## References

[1] "A Energia Solar no Mundo," 2021. https://www.portalsolar.com.br/energia-solar-no-mundo

[2] "Paraíba vai ter fábrica de módulos e novo complexo solar," 2021. https://www.portalsolar.com.br/energia-solar-no-mundo

[3] "Dados do Mercado de Energia Solar do Brasil," 2021. https://www.portalsolar.com.br/mercado-de-energia-solar-no-brasil.html

[4] E. Antolín, M. H. Zehender, P. García-Linares, S. A. Svatek, and A. Martí, "Considerations for the Design of a Heterojunction Bipolar Transistor Solar Cell," *IEEE J. Photovoltaics*, vol. 10, no. 1, pp. 2–7, 2020, doi: 10.1109/JPHOTOV.2019.2945914.

[5] G. Giliberti, A. Marti, and F. Cappelluti, "Perovskite-Si solar cell: A three-terminal heterojunction bipolar transistor architecture," *Conf. Rec. IEEE Photovolt. Spec. Conf.*, vol. 2020-June, pp. 2696–2699, 2020, doi: 10.1109/PVSC45281.2020.9300949.

[6] Q. R. Lai *et al.*, "Photocurrent of MOS-Si photovoltaic device enhanced by an auxiliary biasing solar cell," *Tech. Dig. - 2012 17th Opto-Electronics Commun. Conf. OECC 2012*, no. July, pp. 701–702, 2012, doi: 10.1109/OECC.2012.6276799.

[7] M. R. Siddiqui, M. R. Khan, and M. R. Khan, "A double gate MOS structure for solar photo-voltaic application," *ICECE 2010 - 6th Int. Conf. Electr. Comput. Eng.*, no. December, pp. 734–737, 2010, doi: 10.1109/ICELCE.2010.5700797.

[8] F. L. N. Santos, M. N. Watanabe, W. C. Junior, S. G. D. S. Filho, and J. A. Martino, "Bifacial tandem solar panels with MOS cells on the backside for applications in deserts," *SBMicro 2019 - 34th Symp. Microelectron. Technol. Devices*, pp. 0–3, 2019, doi: 10.1109/SBMicro.2019.8919381.

[9] W. J. Ho, M. C. Huang, Y. Y. Lee, Z. F. Hou, and J. J. Liao, "Demonstration of high efficiency 19.68% MOS-structure silicon solar cell based on 20-nm TiO2 space layer at 4V biasing," *2014 IEEE Int. Nanoelectron. Conf. INEC 2014*, no. 1, pp. 1–3, 2016, doi: 10.1109/INEC.2014.7460324.

[10] M. Dey, M. F. Shahriar, A. Ali, M. Dey, and N. K. Das, "Design and Optimization of an Efficient Molybdenum Disulfide (MoS2) Solar cell with Tin Sulfide BSF," *2nd Int. Conf. Electr. Comput. Commun. Eng. ECCE 2019*, pp. 1–5, 2019, doi: 10.1109/ECACE.2019.8679178.

[11] M. N. Watanabe, W. C. Junior, V. Christiano, F. Izumi, and S. G. Dos Santos Filho, "Fabrication and electrical characterization of MOS solar cells for energy harvesting," *33rd Symp. Microelectron. Technol. Devices, SBMicro 2018*, pp. 18–21, 2018, doi: 10.1109/SBMicro.2018.8511579.

[12] W. J. Ho *et al.*, "Performance enhanced of MOS-structure silicon solar cell based on the integration of photovoltaic biasing source," *2014 IEEE 40th Photovolt. Spec. Conf. PVSC 2014*, pp. 213–215, 2014, doi: 10.1109/PVSC.2014.6925597.

[13] R. S. Sue, W. J. Ho, S. H. Weng, J. C. Lin, and Y. J. Deng, "Photovoltaic Performance Enhancements of MOS-Structure Si Solar Cells Based on Antireflection, Biasing, and Plasmonic Scattering," *Opt. InfoBase Conf. Pap.*, pp. 1–2, 2016.

[14] Jenny A. Nelson, *The Physics os Solar Cells*. Imperial College Press, 2003.

[15] S. P. Gimenez, *Layout Techniques for MOSFETs*. San Mateo, CA, USA: Morgan & Claypool Publisher, 2016.

[16] S. P. Gimenez, D. M. Alati, E. Simoen, and C. Claeys, "FISH SOI MOSFET: Modeling, Characterization and Its Application to Improve the Performance of Analog ICs," *Journal of the Electrochemical Society*, pp. H1258–H1264, 2011. doi: 10.1149/2.091112.

[17] V. V Peruzzi, G. A. Silva, and S. P. Gimenez, "Experimental Comparative Study Regarding the Mismatch Between the FISH nMOSFET and its Conventional Counterparts," 2015.

[18] Synopsys, *Sentaurus Device User Guide*, Versão O-2. 2018.

[19] C. Canali, G. Majni, R. Minder, and G. Ottaviani, "Electron and hole drift velocity measurements in silicon and their empirical relation to electric field and temperature," *IEEE Trans. Electron Devices*, vol. 22, no. 11, pp. 1045–1047, 1975.

[20] D. B. M. Klaassen, "A Unified Mobility Model for Device Simulation-I. Model Equations and Concentration Dependence," *Solid. State. Electron.*, vol. 35, pp. 953–959, 1992.

[21] C. Lombardi, S. Manzini, A. Saporito, and M. Vanzi, "A Physically Based Mobility Model for Numerical Simulation of Nonplanar Devices," *IEEE Trans. Comput. Des. Integr. Circuits Syst.*, vol. 7, no. 11, pp. 1164–1171, 1988, doi: 10.1109/43.9186.

[22] C. Sah, R. N. Noyce, and W. Shockley, "Carrier Generation and Recombination in P-N Junctions and P-N Junction Characteristics," *Proc. IRE*, vol. 45, no. 9, pp. 1228–1243, 1957, doi: 10.1109/JRPROC.1957.278528.

[23] J. G. Fossum and D. S. Lee, "A physical model for the dependence of carrier lifetime on doping density in nondegenerate silicon," *Solid State Electron.*, vol. 25, no. 8, pp. 741–747, 1982, doi: 10.1016/0038-1101(82)90203-9.